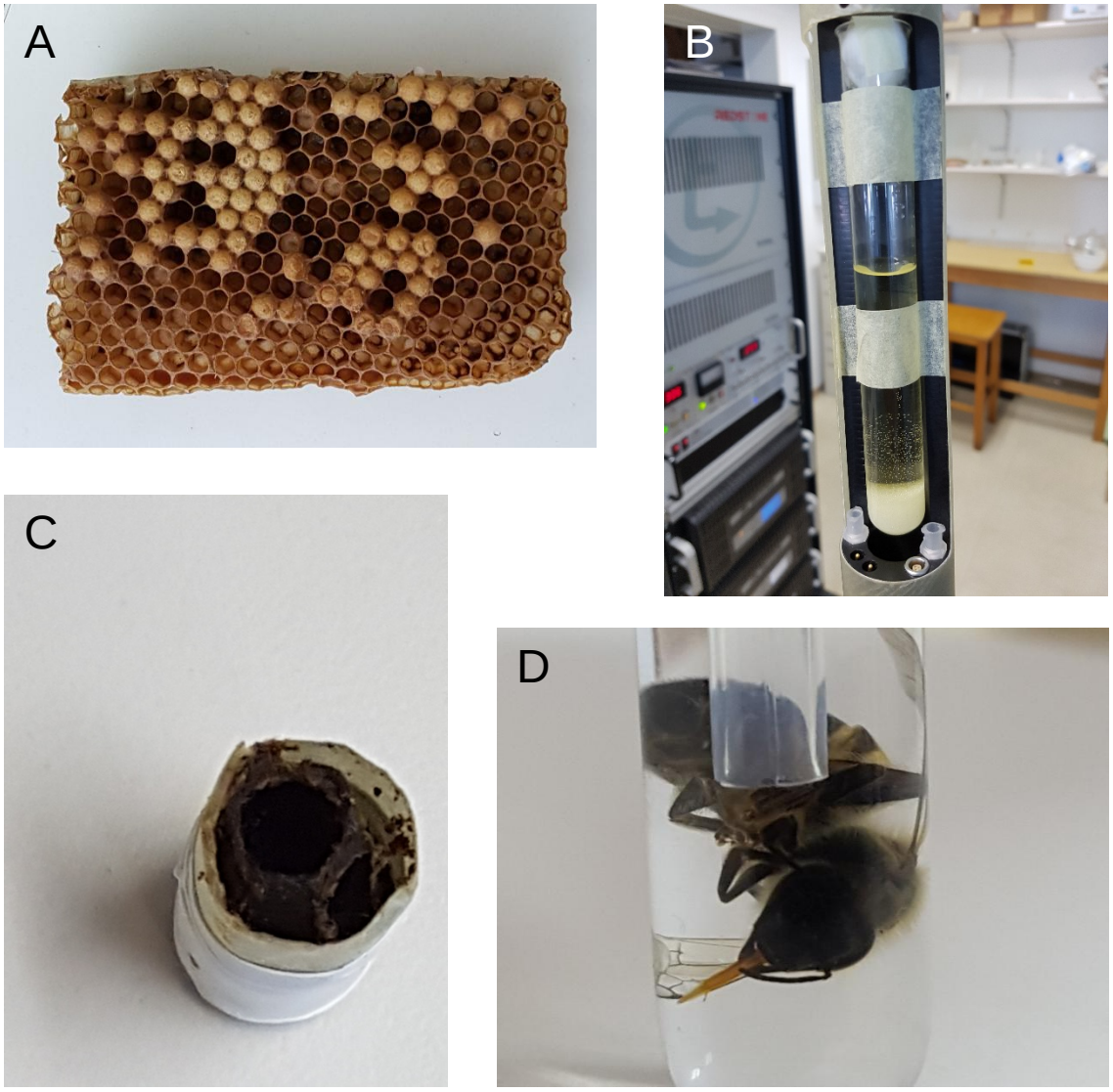

Fig. S1. Experimental setup. The experiment was performed in August 2018, which is an optimal period for bee reproduction. (A) First, a caped cell with a larva was isolated from the honeycomb. Then the cell was truncated to the diameter of 10 mm, wrapped in Teflon tape and inserted in a 10 mm probe for magnetic resonance microscopy (MRM). (B) To maintain optimal humidity of 62 % during the experiment, below the cell a tube filled with a saturated solution of $NaNO_2$ in water was placed. The optimal temperature of 34 °C was maintained during the entire experiment by the MRM probe conditioning system. (C) After twelve and a half days, metamorphosis was completed, and the adult bee emerged from the cell. (D) Adult bee emerging from the glass which was kept for further analysis.

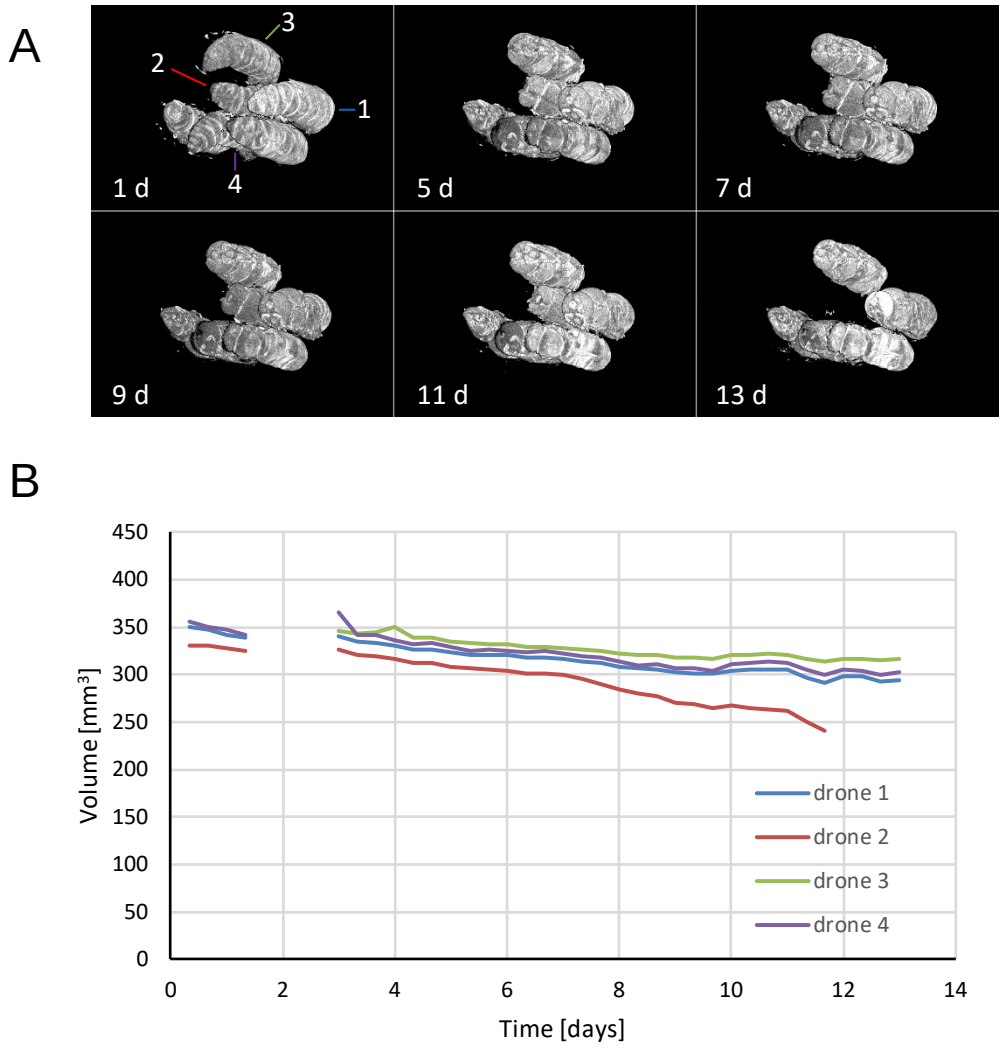

Fig. S2. Development of multiple drones followed by sequential MRM. (A) Volume rendered images of the four developing drones at different time points during metamorphosis. (B) Graph shows the total volume time courses for each of the four different drones. The analyzed drones have indices 1-4 and curves of different colors in the graph. Placing multiple specimen in the imaging field of view enables their simultaneous scanning and therefore enables the statistical analysis of variability among the specimens. This approach is much faster than the traditional approach where each specimen of the group is scanned separately. The drawback for simultaneous multiple scanning is partial loss of spatial resolution.

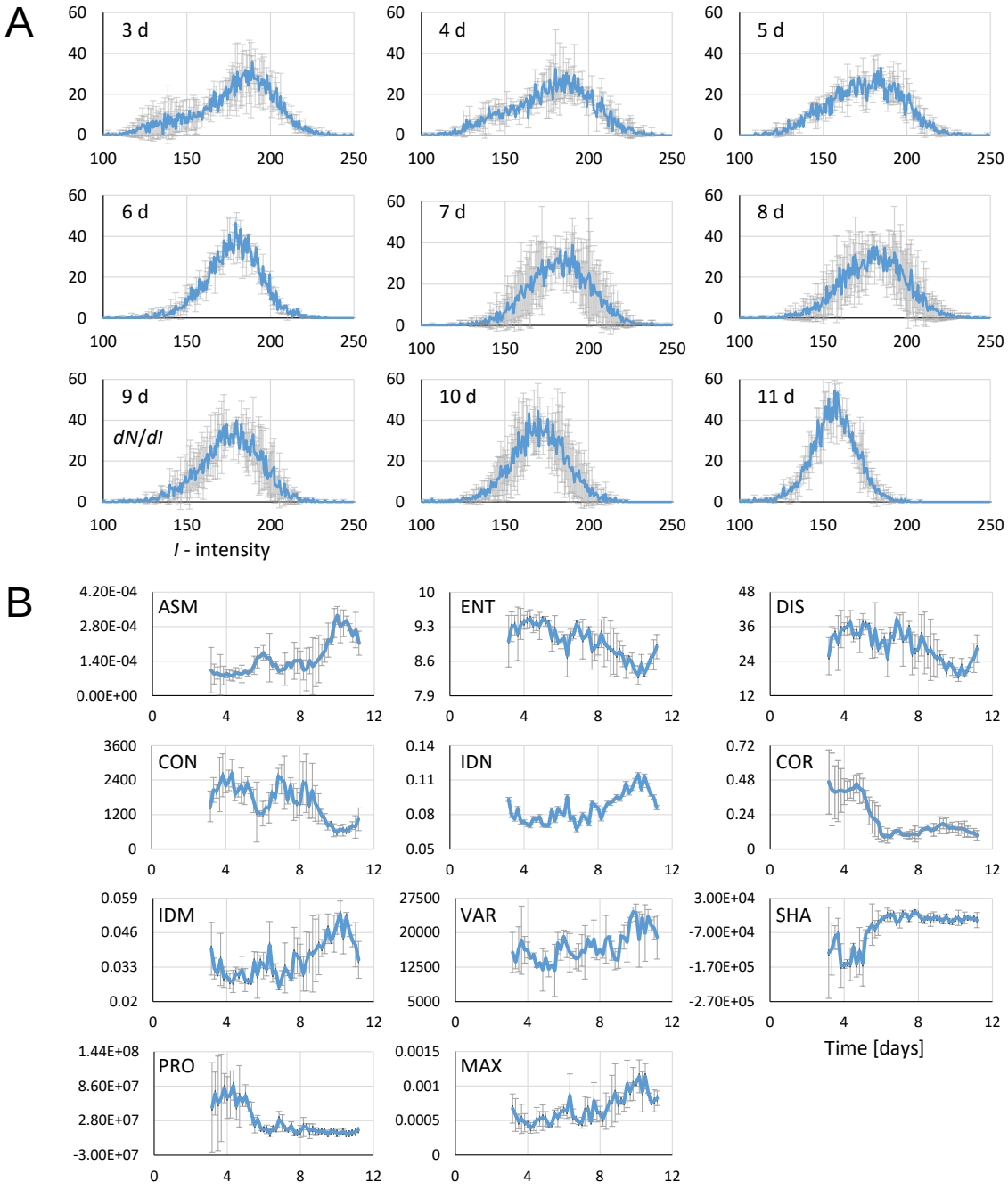

Fig. S3. Compositional analysis and structural analysis of the flight muscle. (A) The selected region of interest (ROI) within the flight muscle are analyzed by image signal histograms of both specimens at one day intervals. The histograms all exhibit approximately normal distributions; however, the distributions have different means and widths. They reveal transformation of the flight muscle composition from the initial fat-rich to the final low-fat content. (B) The selected ROI is analyzed for the structural changes by the gray level co-occurrence matrix (GLCM) analysis. Time courses of all the eleven second-order statistical texture features derived from the GLCM maps are also shown. Some of the features, such as: correlation (COR), cluster shade (SHA), cluster prominence (PRO) and angular second moment (ASM) show a marked dependence on time, while some others, e.g.: entropy (ENT), dissimilarity (DIS), contrast (CON), inverse difference normalized (IDN), inverse difference moment (IDM), variance (VAR) and maximum probability (MAX) are less distinctive.

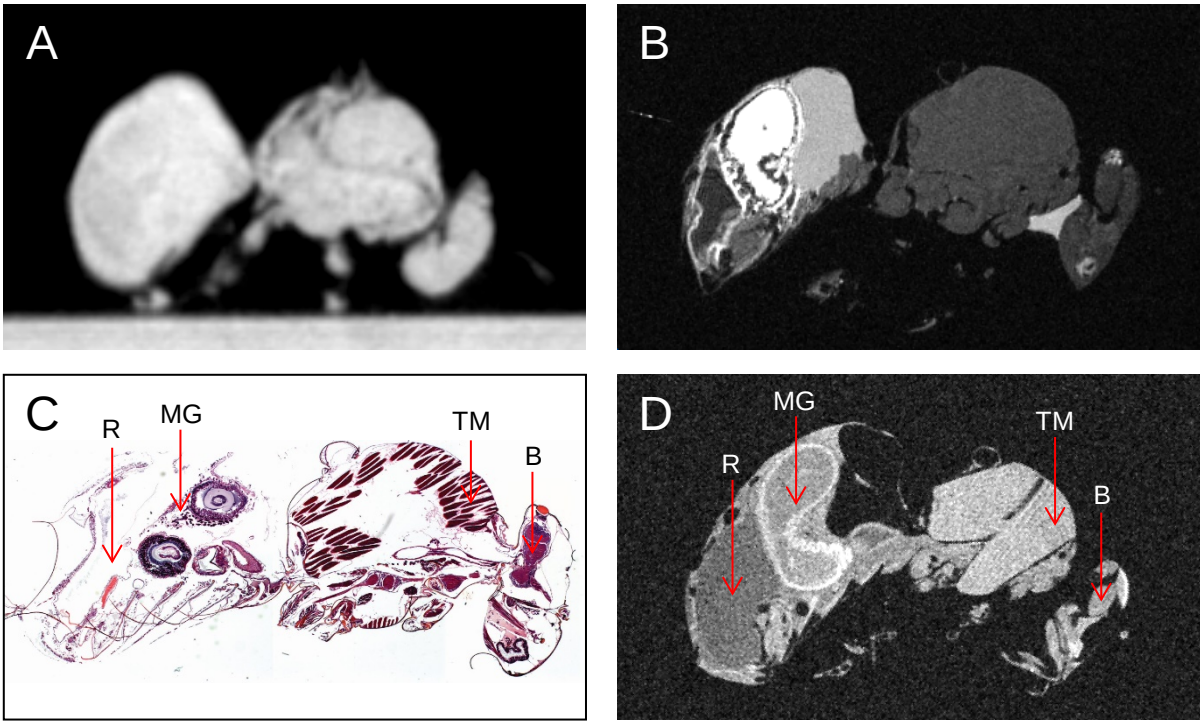

Fig. S4. Comparison between micro CT, microanatomy and MRM images. (A) micro CT and (C) microanatomical images and the corresponding MRM images of the (B) winter and (D) summer worker honey bees in identical slices. Micro CT image was acquired at field of view 40 × 40 × 40 mm^3 and x-ray tube voltage was set at 90 kV, while microanatomical dissection was performed in 7 μm thick sagittal sections that were stained by hematoxylin-eosin following the procedure described in *Microanatomy* subsection. Prior to MRM scanning the samples were immersed in perfluorinated fluid (Galden SV90, Solvay, Brussels, Belgium) to prevent their desiccation during scanning which was performed using a 3D spin-echo T_1-weighetd imaging sequence with parameters TE/TR = 1.9/200 ms, field of view 18 × 9 × 9 mm^3, imaging matrix of size 512 × 256 × 256, four signal averages and scan time of 15 hours. Resolution of MRM images is equal to 35 μm isotropic and is equal to 80 μm in the micro CT image. Comparison of both image types clearly shows much better contrast among soft tissues in the MRM images than in the micro CT image. In the presented case the MRM images are T_1-weighetd and have tissues with higher fat content much brighter than other tissues. Due to better contrast all internal structures and organs can be better seen; it is much harder to see these on the micro CT image. Also, in terms of spatial resolution MRM images are superior and are closer to the microanatomical reference standard than the CT image. However, this is not typical as there are many reports in the literature on micro CT of insects in which approximately an order of magnitude better resolution was obtained. All major anatomical parts that are seen on the microanatomical image can be clearly seen on the corresponding MRM image as well. Specifically, brain (B) in the head, flight muscles (TM) in the thorax, midgut (MG) and rectum (R) in abdomen.

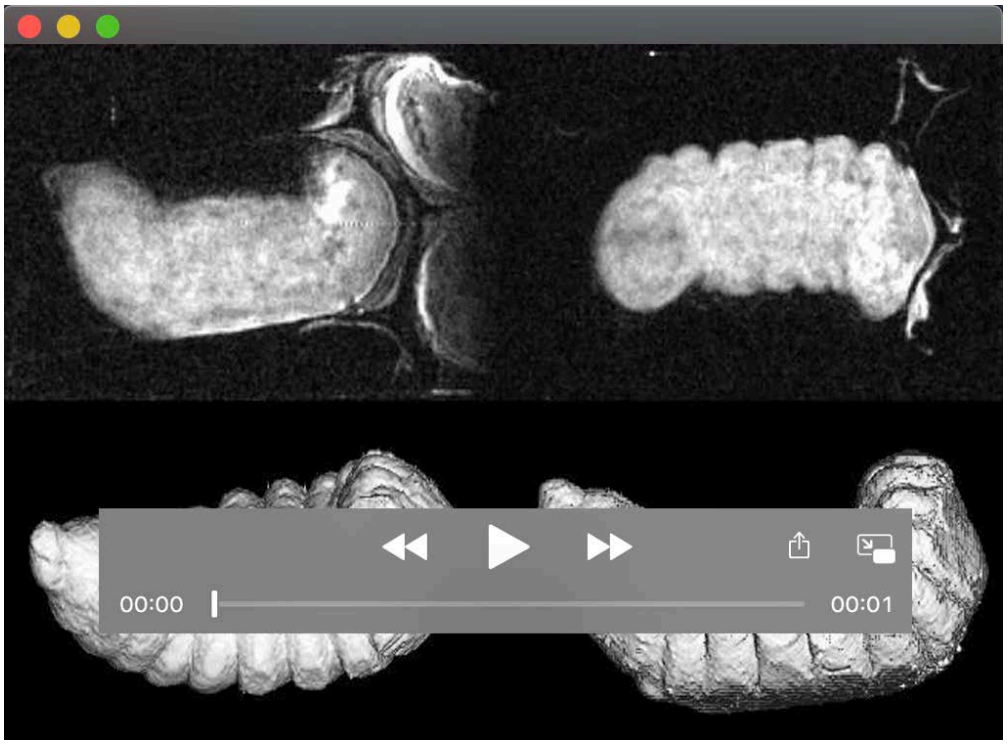

Movie 1. Metamorphosis of the bees in the central slice view and by volume-rendered images. Movies of the (left column) first and the (right column) second worker honey bee shown by: (upper row) the central slice in the sagittal orientation and by (bottom row) volume rendered images. (upper row) The central slice movies provide a clear insight into the structural changes during different stages of metamorphosis. A sudden transformation from larva to pupa was followed by the evident structural changes in the gastrointestinal tract, in the tracheal system and also in many other organs. Spatial resolution of the movies is 78 μm. Bright regions correspond to fat-rich tissues, while the darker regions contain more body fluids; signal void regions contain no tissues. Blurred frames at the end of the movies indicate intense spinning by the pupa. (bottom row) A complete set of all image slices, i.e., a full 3D image also enables the volume rendering of the entire bee. This study was done with the Fiji distribution of the ImageJ digital image processing software on each of the acquired images with the matrix size of 256 × 128 × 128. The movies show worker bee metamorphosis from the sealed larva to the emergence of an adult bee.

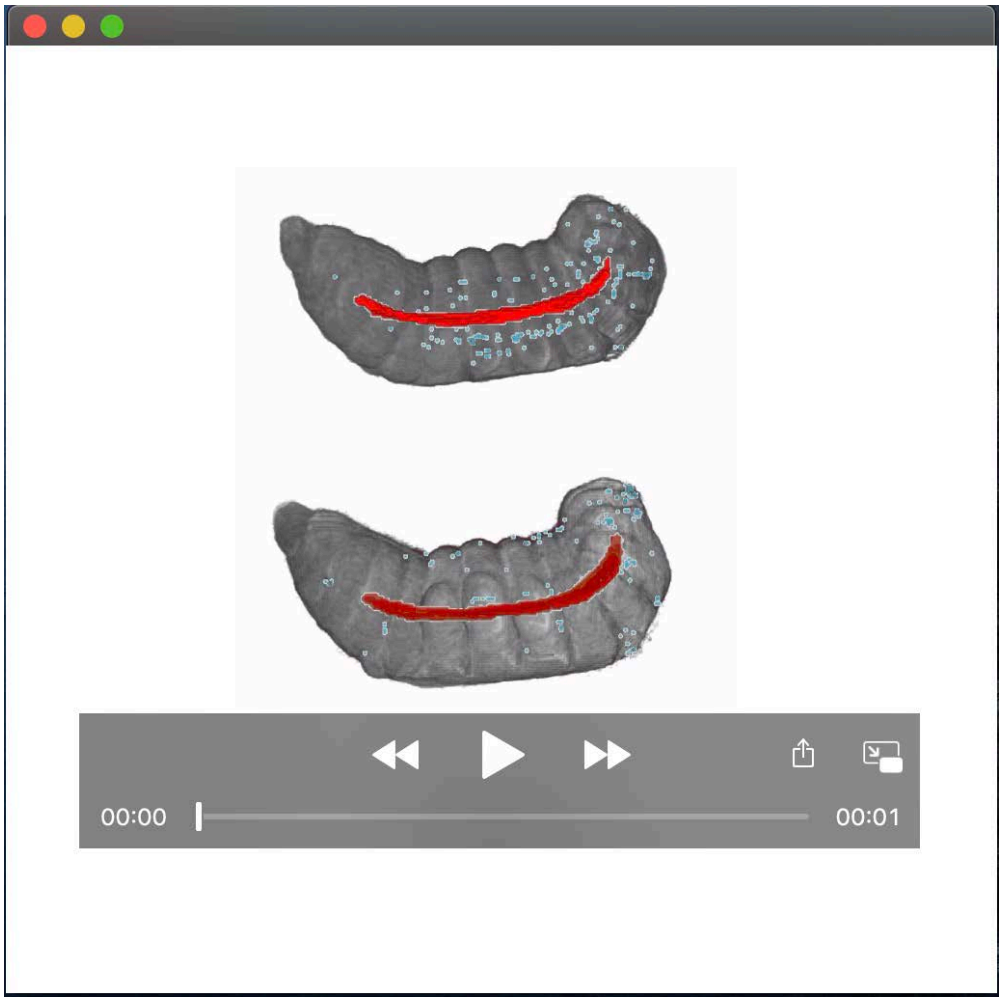

Movie 2. Development of tracheal and gastrointestinal system. Movies of (top) first and (bottom) second worker honey specimens show a time sequence of the volume-rendered images in sagittal view of the segmented organs: gastrointestinal tract is shown in red, honey stomach in orange and tracheal system in blue. In the movies, curvature development of the gastrointestinal tract is clearly visible. The tract can be reduced to a single narrow curve spanning through the entire tract region. The curve enabled measurement of the tract length time dependence as well as the measurement of the distance between the tract end points. This information was needed for the calculation of the tract's tortuosity and its time dependence during the metamorphosis that is shown in Fig 2.